Solid State Ionics 343 (2019) 115072

Contents lists available at ScienceDirect

Solid State Ionics

journal homepage: www.elsevier.com/locate/ssi

Electromechanical losses in carbon- and oxygen-containing bulk AlN single crystals

Iurii Kogut[a,*], Carsten Hartmann[b], Ivan Gamov[b], Yuriy Suhak[a], Michal Schulz[a], Sebastian Schröder[a], Jürgen Wollweber[b], Andrea Dittmar[b], Klaus Irmscher[b], Thomas Straubinger[b], Matthias Bickermann[b], Holger Fritze[a]

[a] Institut für Energieforschung und Physikalische Technologien, Technische Universität Clausthal, Am Stollen 19B, 38640 Goslar, Germany
[b] Leibniz-Institut für Kristallzüchtung, Max-Born-Straße 2, 12489 Berlin, Germany

ARTICLE INFO

Classification codes:
A60
A70*Keywords:*
Aluminum nitride
Bulk acoustic wave resonator
Electromechanical losses
Anelastic relaxation of point defects

ABSTRACT

Bulk single-crystalline aluminum nitride (AlN) is potentially a key component for low-loss high-temperature piezoelectric devices. However, the incorporation of electrically active impurities and defects during growth of AlN may adversely affect the performance of piezoelectric resonators especially at high temperatures. The electrical conductivity and electromechanical losses in bulk AlN single crystals are analyzed in the temperature range of 300–1200 K with respect to various contents of growth-related impurities in them. For AlN with [O]/[C] ≤ 1, an increase of electrical conductivity due to thermal activation of charge carriers in the temperature range of 850–1200 K has been observed and was determined to be a major contribution to electromechanical losses Q^{-1} rising up to maximum values of about 10^{-3} at 1200 K. As the oxygen content in AlN increased, the magnitude and the activation energy of high-temperature electrical conductivity increased. In oxygen-dominated AlN, two major thermally activated contributions to electromechanical losses were observed, namely, the anelastic relaxations of point defects at temperatures of 400–800 K and electrical conductivity at $T > 800$ K.

1. Introduction

Successful implementation of piezoelectric materials in resonant devices, in particular for high-temperature applications, requires that they are structurally and chemically stable, possess minimum electrical conductivity and contain least possible intrinsic defects, unless intentionally introduced for compensation of other defects. Bulk single crystalline aluminum nitride (AlN) is expected to meet these essential requirements and is, perhaps, a key material for use in high-temperature piezoelectric resonators [1], e.g. in micro- and nanobalances, thin film calorimeters, pressure sensors in aircraft turbojet engines, motors, temperature sensors, etc. However, due to difficulties in producing large high-quality single crystals, in the past several decades the research has been mostly focused on the device integration of thin-film AlN piezoelectric resonators [2–7].

Aluminum nitride single crystals exhibit a wurtzite-type symmetry, which is a thermodynamically stable phase showing no transitions up to the melting point. The latter varies within 2473–3427 K depending on the nitrogen pressure in the environment [1,8,9]. The existence of metastable rocksalt AlN phase has been reported, but its formation required strains on the order of tens GPa and extreme temperatures far beyond the ranges of anticipated operation for AlN-resonators [10–12] and experimental characterization in this work. The metastable zinc-blende AlN can be stabilized only by heteroepitaxial growth of very thin films on certain planes of cubic substrates [9]. Noteworthy, the centrosymmetric cubic crystal structure of both these phases do not show the piezoelectric effect.

Other important aspects to consider are oxidation and thermal shock resistance. As the surface primarily degrades at the presence of oxygen until formation of passivating oxide scale [8,13], bulk acoustic wave (BAW) devices are usually less affected [14] than the thin-film based ones [2] and, consequently, AlN-based BAWs are preferred in oxygen containing atmospheres for operation at high temperatures. Further, owing to high thermal conductivity [15,16], AlN is also resistant to thermal shocks.

For comparison, in context of structural stability and high-temperature piezoelectric applications, lithium niobate and related compounds suffer from evaporation of lithium (sub)-oxides or Curie temperatures that limit their application in piezoelectric resonators [17,18]. The piezoelectric crystals of the langasite group are

* Corresponding author.
E-mail address: iurii.kogut@tu-clausthal.de (I. Kogut).

https://doi.org/10.1016/j.ssi.2019.115072
Received 1 May 2019; Received in revised form 17 September 2019; Accepted 18 September 2019
Available online 06 November 2019

thermodynamically stable up to the melting point (1600–1800 K [19]), but the high-temperature applications of some crystals may be obscured by the relatively high electrical conductivity, e.g. the $La_3Ga_5SiO_{14}$ (LGS) exhibits conductivity as high as 10^{-2}–10^{-3} S/cm due to occurrence of oxygen ion transport in the temperature range of 1000–1300 K [19–23]. Other crystals of the langasite family exhibit lower conductivity, which is, however, reported to be higher than that of AlN [24].

Meanwhile, intrinsic electric conductivity in the range of 10^{-10}–10^{-11} S/cm at T = 1100–1300 K has been reported for nominally undoped AlN single crystals [24]. However, despite the recent progress in fabricating of relatively large AlN single crystals of high structural perfection, gained by the seeded growth in the physical vapor transport (PVT) process [25–31], the incorporation of dislocations, electrically active impurities and native point defects [28–38] may be detrimental to their insulating and electromechanical properties. In this concern, especially the control of impurities incorporation upon PVT growth of AlN remains a challenging task [30]. These impurities are majorly carbon and oxygen with some traces of silicon, which are inevitable residuals from the carbothermal reduction and subsequent purification of AlN starting material [39]. Carbon and traces of Si originate also from the hot-zone parts in growth chamber, i.e. TaC crucibles that partly decompose in Ta_2C and C at temperatures above 2500 K or higher [26]. Oxygen is mainly sourced by the alumina contained in starting AlN material, which is a consequence of high affinity of Al for oxygen [30,31].

The type and concentration of named impurities determine the configuration of point defects in AlN and, therefore, its electrical, electromechanical and optical (e.g. coloration) properties. Carbon is a deep acceptor impurity in AlN, substituting on nitrogen sites and forming the acceptor-donor pairs with compensating nitrogen vacancies [37,40–42]. Electrical conductivities with activation energies E_a in the range of 1.8–2.0 eV at T = 900–1300 K were reported for carbon-dominated AlN [40,43]. The electrical conductance of oxygen-dominated AlN occurring yet at moderate temperatures of 300–700 K is attributed to generation of extrinsic electrons by a donor reaction involving substitutional oxygen atoms on nitrogen sites [44–51]. The related increase in activation energy of conductivity (slightly above 2 eV) is consistent with the increase of O concentration and formation of defect complexes with compensating aluminum vacancies [45–49]. The charged $V_{Al}''' - 3O_N^{\bullet}$ complexes were speculated to cause thermally activated electrical and mechanical anelastic relaxations peaking at 1223 K and 623 K in polycrystalline dense packed AlN [52]. Finally, while silicon is an electrically active impurity in AlN, its incorporation during PVT growth usually results in only trace concentrations (few ppms), which are considered insufficient, in particular in the present study, for influencing AlN properties [30,31].

Although extensive research on incorporation of electrically active impurities and formation of point defects in single crystalline AlN has been performed, to our knowledge, no studies with special consideration of their influence on electromechanical properties of bulk AlN resonators have been published so far. Hence, the present research aims on the identification of factors that contribute in the high-temperature electrical conductivity and electromechanical losses in piezoelectric AlN bulk single crystals, depending on the concentration of growth-related oxygen and carbon impurities in them.

2. Experimental methods and fundamental sample properties

2.1. Fundamental properties and preparation of studied AlN samples

The investigated bulk AlN single crystals were grown at Leibniz-Institut für Kristallzüchtung (Berlin, Germany) by physical vapor transport. The crystals grew along the [0001] direction (*c*-axis) in the form of 6 to 15 mm long hexagonal prisms with diagonals of 7 to 12 mm (Fig. 1, *a*). Details on the PVT growth method and resulting structural

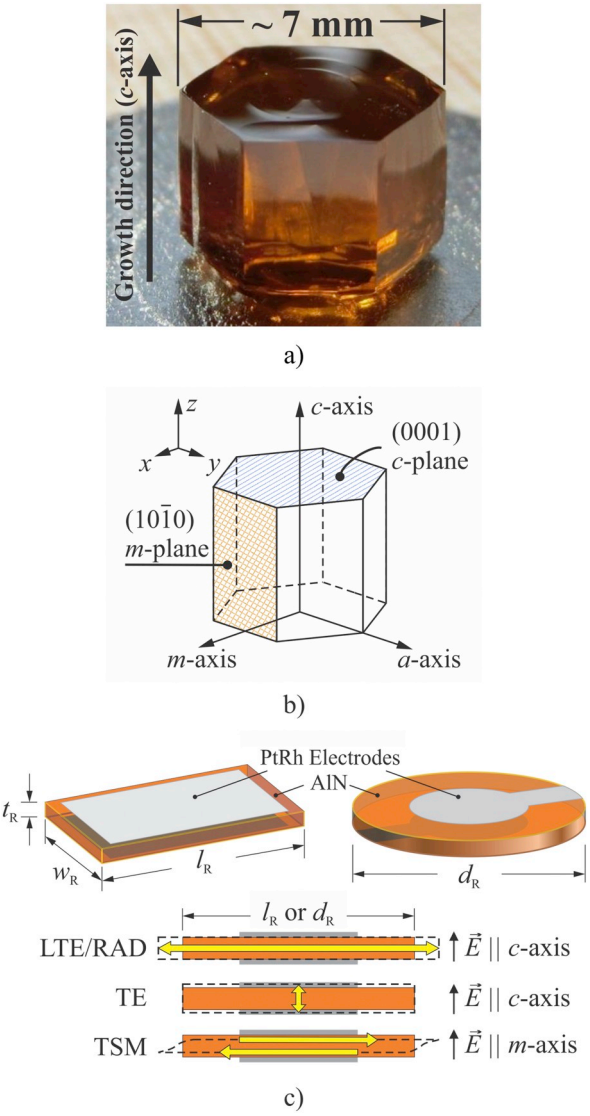

Fig. 1. A PVT-grown AlN single crystal (*a*), schematic view of the AlN wurtzite-type single crystal (*b*), and a typical design of AlN resonators (*c*) with keyhole-shaped and rectangular electrodes center-aligned with either *c*- or *m*-axes in the middle of the resonator. The orientation of applied alternating electrical field $\vec{E}$, exciting different resonant modes, is shown on the right, and yellow arrows depict the oscillation directions in each mode. (For interpretation of the references to colour in this figure legend, the reader is referred to the web version of this article.)

quality and native defects of the studied AlN crystals are provided in [26,31]. The concentrations of oxygen and carbon in the studied samples were determined by secondary ions mass spectroscopy (SIMS) and provided in Table 1. The uncertainty of determined concentrations of oxygen and carbon impurities in AlN did not exceed 10%. Depending on the domination of either O or C, the AlN samples differed in coloration as also noted in Table 1.

For sake of clarity, a naming scheme for studied samples will be used with prefix ("c-" or "m-"), indicating the crystal's orientation, and capital letters "O" or "C" pointing on the dominant impurity in the sample followed by a plus sign indicating on high concentration of the impurity (with "OC" meaning nearly equal concentrations of O and C).

In addition, a nearly colorless 550 µm thick (0001)-AlN single crystal was purchased from HexaTech Inc. (Morrisville, North Carolina, USA) and used for reference measurements (c-OC+ in Table 1).

Rectangular and disk-shape *c*-cut (0001) plates (Fig. 1, *b*) were

Table 1
Description of the studied AlN samples.

Sample name	Coloration	Impurity concentration (mol. ppm)		Shape	Dimensions (mm)			Cut (Fig. 1, *b*)	Excitation modes
		[C]	[O]		l_R or d_R	w_R	t_R		
m-C+	Amber	68	28	Circular	9.00	–	0.80	$(10\bar{1}0)$	TSM
c-C	Bright amber	31	22	Rectangular	7.80	5.70	0.76	(0001)	LTE; TE
c-OC	Colorless	27	27	Circular	5.02	–	0.76	(0001)	RAD; TE
c-OC + (Ref.)	Colorless	94	94	Rectangular	8.00	6.00	0.55	(0001)	LTE; TE
c-O	Brownish	17	29	Rectangular	6.02	4.98	0.75	(0001)	LTE; TE
c-O+	Pale yellowish	19	77	Circular	4.87	–	0.53	(0001)	RAD; TE

Note: the column "Cut" means, that the largest face of the AlN plate is parallel to the indicated plane (Fig. 1, b).

sliced from as-grown bulk AlN. The sample dimensions are given in Table 1. The length-thickness extensions (LTE) were excited in rectangular (0001)-AlN samples with length l_R larger than width w_R, whereby both l_R and w_R were much larger than resonator's thickness t_R. Resulting from *6mm* symmetry of hexagonal crystal lattice of AlN, in circular (0001)-oriented resonators with diameter $d_R \gg t_R$ the LTE couples to a radial oscillation mode (RAD). Also thickness extensions (TE) were observed in the (0001)-AlN plates of both shapes. The *m*-cut $(10\bar{1}0)$-AlN disks ($d_R \gg t_R$, Fig. 1, *b*) were used for excitation of thickness-shear mode (TSM).

Room-temperature materials data for AlN, the elastic compliances c_{mn} and the density ρ, used, in particular, for calculation of resonance frequencies in Section 3.2.1 were taken from [53] and were as follows: $c_{11} = 402.5$ GPa and $c_{12} = 101$ GPa (used for RAD and LTE), $c_{33} = 387.6$ GPa (RAD and TE), $c_{44} = 122.9$ GPa (TSM), and $\rho = 3260\ \mathrm{kg/m^3}$.

After cutting, the AlN plates were polished on both sides, and either keyhole-shaped or rectangular (Fig. 1, *c*) ~200 nm thick Pt-Rh electrode layers with 10 nm Ti adhesive layer beneath were applied by pulsed laser deposition on both faces of the plates. The deposited electrodes were center-aligned with the studied plate along the *c*- or *m*-axes.

2.2. Measurement methods

For the measurements of temperature dependences of electrical and resonant properties of AlN in the temperature range of 300–1200 K, the samples were placed between the platinum foil contacts of electrical signal feed lines in an alumina holder, and the setting was heated in the furnace at a rate of 1 K/min. To minimize oxidation of AlN, the furnace was steadily purged with flowing argon (purity > 99.996%; 20 $\mathrm{cm^3}$/min) during the measurements.

The electrical impedance spectra (EIS) of AlN were measured using the afore-mentioned fixture and the Solartron SI 1260 impedance spectrometer, assisted by the high-impedance measuring bridge Solartron SI 1296. The $Z''(Z')$ dependences were swept within frequency range of 1–10^6 Hz with an excitation AC voltage of 0.05–0.2 V. Here Z'' and Z' are the imaginary and the real part of sample's impedance, respectively. Temperature deviation within one EIS sweep did not exceed ± 3 K. The electrical properties of AlN samples were modeled with an electrical equivalent circuit, consisting of bulk resistance R_B in parallel to constant phase element (CPE). Least squares fitting of model parameters to measured EIS allowed for derivation of the bulk resistance R_B of AlN, and the electrical conductivity $\sigma_B(T)$ was extracted from R_B using the dimensions of Pt-Rh electrodes and thickness t_R of the sample.

The resonance spectra of AlN samples were acquired by resonant piezoelectric spectroscopy [54,55] using a high-speed network analyzer Agilent E5100A. Temperature dependences of resonance frequencies f_r and *Q*-factors of AlN resonators in each oscillation mode were obtained by Lorentz-fit of sample's conductance *G* in the vicinity of resonance frequency as a function of frequency *f* in accordance with bandwidth approach to evaluation of resonator quality factor [54]:

$$G(f) = \frac{2A}{\pi}\frac{\Delta f}{4(f - f_r)^2 + \Delta f^2}, \quad (1)$$

$$Q = \frac{f_r}{0.64\Delta f}. \quad (2)$$

In Eqs. (1) and (2) Δf is the bandwidth at half-maximum of conductance and *A* is an adjustable fitting parameter. The factor *0.64* reflects the dependence of the quality factor on energy, which is proportional to G^2. Temperature fluctuations during one cycle of resonance spectra acquisition within about 1 s were negligible.

Note that in some cases of measurements at fundamental tones for TE and TSM artefacts such as several resonance peaks in the vicinity of f_r occurred on the resonance spectra, whereas "clean" single-peak features were observed for higher odd harmonics. These artefacts, in particular for TE mode of disc plates, can be explained by the contribution from spurious modes with flexural components that excite in the crystal with limited dimensions, when the acoustic wavelength is a greater fraction of resonator's lateral dimensions [56–58]. As a result of coupling with spurious modes upon measurements at fundamental tones the bandwidth approach tends to yield apparently larger Δf values and, hence, false *Q*-factors. Measurements at higher overtones allow for avoiding the described artefacts [59]. Therefore, the analysis of electromechanical losses in AlN excited to TE and TSM will hereafter pertain only to measurements at higher harmonics (Section 3.3).

Fairly "clean" single-peak resonance spectra were measured at fundamental tone of LTE and RAD modes for all samples, whereas for TE and TSM modes up to three odd overtones could be well distinguished.

Data acquisition during the EIS and resonant spectra measurements was performed by means of in-house made software for SI 1296 and E5100A, respectively. Fitting algorithms, implemented in the in-house made program according to the approach described in [54,55], were used for the extraction of relevant AlN properties (bulk resistances, CPE parameters, resonance frequencies and *Q*-factors) from the measured data.

3. Results and discussion

3.1. High-temperature electrical conductivity of AlN

Temperature dependences of electrical conductivity for the studied AlN plates are plotted in a semi-log scale as functions of inverse temperature in Fig. 2. The behavior and magnitude of $\sigma_B(T)$ for c-OC sample are comparable to those of the reference sample c-OC+. Among the studied samples, both are colorless having [O]/[C] = 1 and exhibit the lowest electrical conductivity in the temperature range of 900–1200 K. Slightly higher conductivities were observed for carbon-dominated AlN m-C+ and c-C, whereby the magnitude of conductivity increased with oxygen content. Considerably higher electrical conductivity (up to two orders of magnitude in c-O) was observed in oxygen dominated AlN. Note, that due to limited availability of *m*-cut AlN samples in the performed study, no statement on the possible influence of the anisotropy of hexagonal Wurtzite-type structure of AlN on the electrical

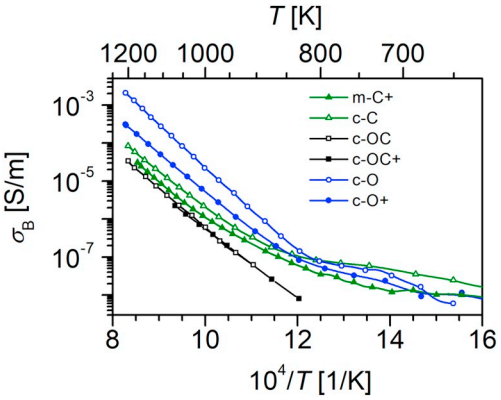

Fig. 2. Temperature dependences of electrical conductivity for bulk AlN samples.

conductivity can be currently made.

A substantial difference in the slopes of $\sigma(T)$ dependences at moderate ($T < 800$ K) and elevated temperatures ($T = 800$–1200 K) is evident, showing a sharp change for oxygen-dominated samples at about 800 K and a much smoother transition occurring at 800–900 K for AlN with lower O content. This observation suggests the change of conductance mechanisms in AlN. In order to determine the activation energies E_a for the clearly distinct conductance mechanisms, the $\sigma_B(T)$ dependences, assuming an Arrhenius form

$$\sigma_B(T) = \sigma_0 \exp \frac{-E_a}{k_B T}, \tag{3}$$

were fitted in the high- and moderate-temperature ranges. Given the overlapping temperature ranges for the charge transport mechanisms in m-C+ sample in Fig. 2, this curve has been fitted by a sum of two Arrhenius functions. The same approach has been tested for all other samples, but the activation energies remained virtually unchanged. Therefore, the modeling with two independent Arrhenius functions has been retained for these samples as it is advantageous to attribute the activation energies to distinct temperature ranges. The obtained values for pre-exponential factors σ_{0i} and activation energies E_{ai} are gathered in Table 2.

The derived E_{a1} within ± 10% of 2 eV in the high-temperature range are in good agreement with literature data, where activation energies of 1.82–2 eV were attributed to carbon impurity [40,43], whereas their rise to 2.2 eV [51] and even higher values was attributed to the increase in oxygen content [46].

Considering the samples m-C+, c-C, c-OC and c-O one can observe a trend towards increasing of the electrical conductivity and its activation energy with [O]/[C] ratio. Worth noting little of analysis of electrical conductivity of single crystalline AlN has been published so far. However, the assumption on conductance origins in the studied AlN can be made based on the data for polycrystalline AlN. In [60] the manifestation of electrical conductivity of polycrystalline AlN at high temperatures in the range of 873–1473 K has been associated with intrinsically generated aluminum vacancies V_{Al}''' that form due to incorporation of oxygen (precipitation of Al_2O_3) in AlN grains. As the concentration of alumina precipitates increased, the amount of Al vacancies also increased, and the activation energy E_{a1} of conductivity rose up to the values of ca. 2.5 eV. Likewise, the conductivities with activation energies E_{a2} in the range of 0.37–0.78 eV at moderate temperatures were reported for AlN and attributed to the formation of aluminum vacancy – oxygen defect complexes [38,52,61]. However, no statement can be currently made in regard of strong deviation of the reference sample c-OC+ and sample c-O+ from the observed tendency. Potentially, the Al_2O_3 precipitates could have hindered the electrical transport in oxygen-dominated AlN [60], which appears to be the case for c-O+, but the decrease of E_{a1} is puzzling. Furthermore, equal and overall much higher concentrations of O and C were measured for the c-OC+ reference sample as compared to the other samples, and high [O]/[C] ratio was measured for c-O+. Currently, the observation cannot be explained. Further investigations of AlN intentionally doped with oxygen would be required for clarification of the observed behavior.

It should be noted that the values of high-temperature electrical conductivity for nominally undoped AlN single crystal manufactured by HexaTech, Inc. as presented in [24] were by several orders lower than that in the present study.

3.2. Electromechanical properties of bulk AlN single crystals

3.2.1. Resonance spectra of bulk AlN plates

Resonance spectra of AlN samples have been recorded at temperatures of 300–1200 K for fundamental tones of LTE, RAD, TE and TSM modes as well as for higher odd harmonics of TE and TSM. The expected resonance frequencies for LTE, TE and TSM oscillations can be roughly estimated [59] using the relevant plate dimensions and elastic compliances c_{mn} of AlN (see Section 2.1):

$$f_{r0} = n \frac{1}{2x} \sqrt{\frac{c_{mn}}{\rho}}, \tag{4.1}$$

where x is either l_R (LTE) or t_R (TE, TSM), and n is an odd harmonic number. Rough estimations of f_{r0} for radial oscillations of disc plates account for Poisson's effect [59,62,63] and involve the planar elastic modulus $c_{11}^p = \left(c_{11} - \frac{c_{12}^2}{c_{33}}\right)$ and resonance wave number η_r, corresponding to the planar Poisson's ratio of AlN ($\sigma^p \approx 0.22$ [9,64]; $\eta_r = 1.9977$ [59,62]) for calculations [62,63]:

$$f_{r0} = \frac{\eta_r}{\pi d_R} \sqrt{\frac{c_{11}^p}{\rho}}. \tag{4.2}$$

The harmonics multiplier for RAD is not integer and depends on σ^p [59]. Note that only fundamental tone of RAD oscillations is considered in the present study. The room temperature values f_{r0} of experimental resonance frequencies (Table 3) were consistent with those theoretically predicted from Eqs. (4.1)–(4.2).

Typical look of obtained resonance spectra is provided in Fig. 3. With increasing temperature, the resonance frequencies in all modes dropped monotonically by up to 2.5% (Fig. 4), obeying the parabolic law $f_r(T) = f_{r0} + aT + bT^2$. The parameters a and b were determined by fitting a parabola with temperature dependence of resonance frequencies (Table 3).

Table 2
Activation energies and preexponential factors of electrical conductivity in bulk AlN single crystals at high and moderate temperatures.

Sample name	Temperature range (K)	E_{a1} (eV)	σ_{01} (kS/m)	Temperature range (K)	E_{a2} (eV)	σ_{02} (μS/m)
m-C+	600–1175	1.75 ± 0.15	1.4 ± 0.3	–	0.28 ± 0.03	1.5 ± 0.6
c-C	900–1200	1.90 ± 0.10	14.0 ± 1.3	650–800	0.39 ± 0.08	47.9 ± 8.7
c-OC	950–1200	2.03 ± 0.12	25.0 ± 2.6	–	–	–
c-OC+ (Ref.)	875–1075	1.76 ± 0.12	1.3 ± 0.2	–	–	–
c-O	850–1200	2.24 ± 0.14	8650 ± 820	700–810	0.42 ± 0.11	31.9 ± 6.3
c-O+	850–1200	2.03 ± 0.13	88.1 ± 5.5	650–800	0.45 ± 0.11	32.0 ± 9.1

Table 3
Theoretical and experimental resonance frequencies in fundamental mode of LTE, RAD, TE and TSM for AlN resonators at $T = 300$ K.

Sample name	Mode	x (mm) (Fig. 1, b)	f_{r0} (MHz)		Fit parameters for $f_r(T) = f_{r0} + aT + bT^2$	
					a	b
			Calculation	Experiment	K^{-1}	K^{-2}
m-C+	TSM	$t_R = 0.80$	3.83	3.91	−78.94	−0.015
c-OC	RAD	$d_R = 5.02$	1.36	1.42	−29.27	−0.008
	TE	$t_R = 0.76$	7.45	7.42	−142.93	−0.05
c-OC+ (Ref.)	LTE	$w_R = 6.00$	0.93	0.93	−15.44	−0.006
	TE	$t_R = 0.55$	9.91	9.67	−283.67	−0.006
c-O	LTE	$l_R = 5.00$	1.11	1.13	−25.57	−0.001
	TE	$t_R = 0.71$	7.67	7.55	−169.34	−0.04
c-O+	RAD	$d_R = 4.87$	1.40	1.45	−43.95	−0.001
	TE	$t_R = 0.53$	10.29	10.34	−324.23	−0.015

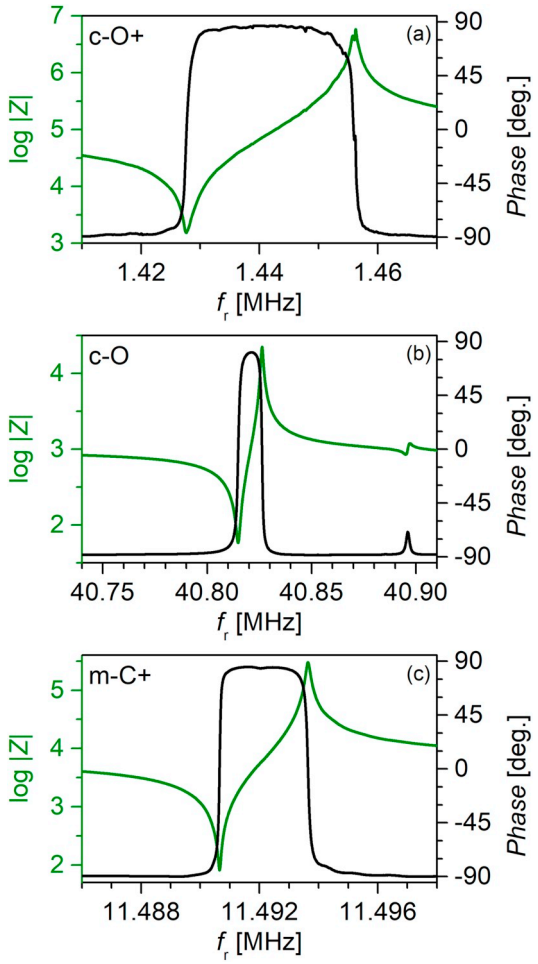

Fig. 3. Room-temperature resonance spectra for sample c-O+ at fundamental mode of RAD (a), c-O at fifth harmonic of TE mode (b), and sample m-C+ at third harmonic of TSM (c).

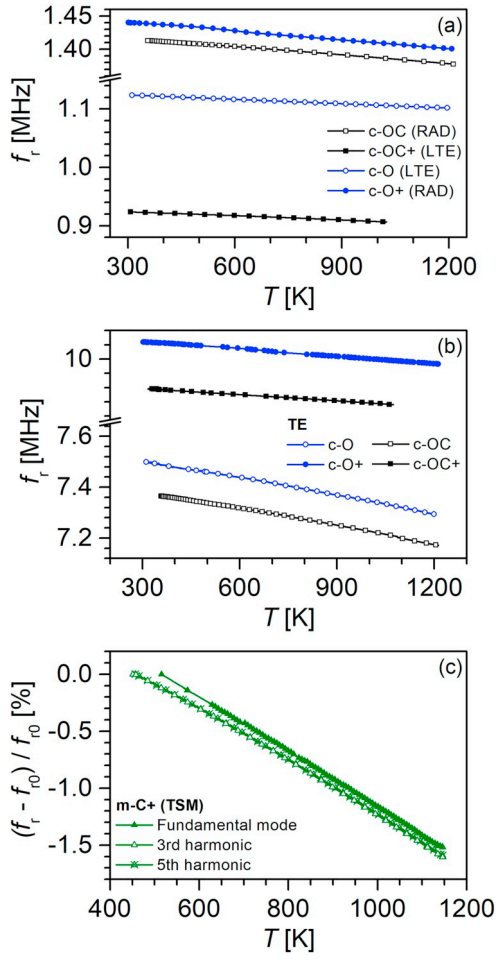

Fig. 4. Temperature dependences of resonance frequency for AlN resonators in (a) LTE and RAD modes, (b) TE mode and (c) relative change of f_r for m-C+ in TSM.

3.2.2. Electromechanical losses in AlN

For implementation in high-temperature resonant devices, the piezoelectric material must exhibit lowest possible attenuation of its electromechanical properties within the anticipated range of operation temperatures. The figure-of-merit expressed as the product of quality factor Q and frequency f represents a parameter that enables comparison of resonators. As the frequencies are in the same order of magnitude for each mode, the discussion of losses can be done using solely the inverse quality factor (Q^{-1}). Hence, the temperature dependences of Q^{-1} were evaluated in order to identify the major contributions to

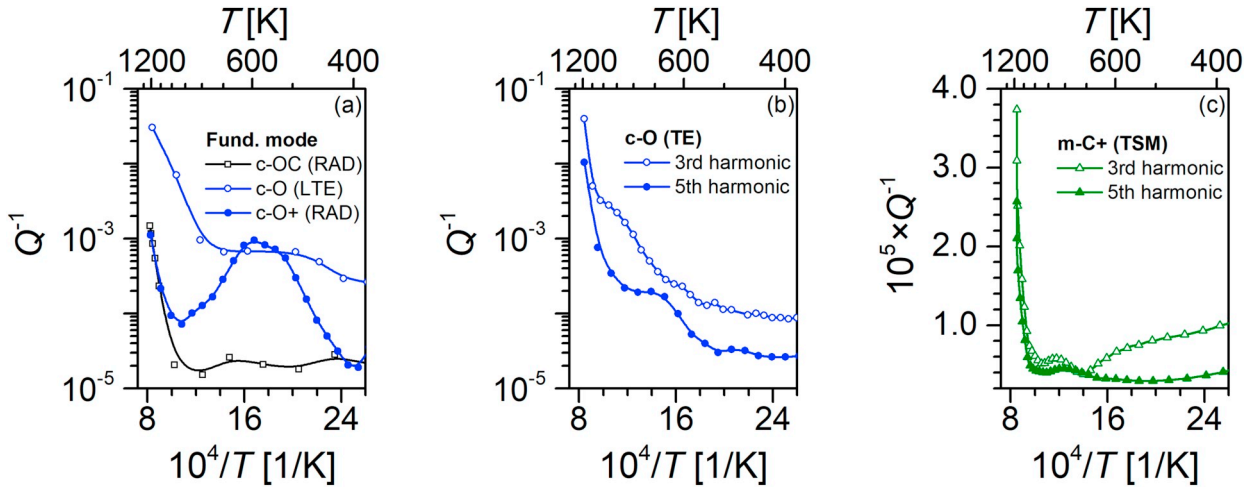

Fig. 5. Electromechanical losses in bulk AlN single crystals at high temperatures: (*a*) fundamental LTE and RAD modes and (*b*) higher harmonics of TE mode for *c*-O, and (*c*) 3rd and 5th harmonics of TSM for *m*-C+ AlN.

electromechanical losses in the studied bulk AlN single crystals with respect to known electrically active impurities (Fig. 5).

Overall the Q^{-1} values in fundamental resonance modes (f_r = 0.9–1.5 MHz in LTE or RAD) are rather high at temperatures below 800–900 K for all samples. However, in comparison to c-O exhibiting $Q^{-1} \sim 10^{-3}$ (LTE, 1.1 MHz), an order of magnitude lower Q^{-1} were observed for carbon-rich AlN, yielding down to $\sim 10^{-5}$ for c-OC (RAD, 1.4 MHz). Likewise, Q^{-1} at higher harmonics show that samples with low [O]/[C] ratios, featuring electromechanical losses as low as $Q^{-1} \approx 3 \times 10^{-6}$ (5th harmonic, f_r = 19.2 MHz, m-C+, Fig. 5, *c*), would be preferred for AlN-based resonators.

Analyzing the results depicted in Fig. 5, important features are worth emphasizing:

1) Steep rise of electromechanical losses at $T > 1000$ K for m-C+ and c-OC and yet at T of 700–900 K for oxygen dominated samples c-O and c-O+.
2) Multi-peak feature with high-temperature Q^{-1} peak at $T > 900$ K and strong and broad peaks on $Q^{-1}(1/T)$ at T = 400–900 K, observed in AlN with increased oxygen content, where the latter suggest anelastic relaxation of defects in AlN [52,65,66].

3.3. Analysis of loss contributions in electromechanical properties of AlN

Reverting to above-emphasized features of the temperature dependences of inverse *Q*-factors, one should first recall a basic concept of an anelastic relaxation in solids, which is essentially a thermodynamic phenomenon of the time-dependent equilibration of body's state in response to external influences. The magnitude of such a change is linear with the exerted force, and the solid fully recovers its state upon removal of the influence (i.e., the solid retains elasticity). The change or recovery, however, are not instantaneous and proceed via certain internal variables that attain new equilibrium values only at a finite rate. This behavior can be, thus, interpreted as an internal friction in the matter. In particular, anelasticity originates from crystal imperfections, such as point defects, dislocations and other crystal defects. The theory of anelastic relaxation in crystalline solids has been extensively described in [65], and was confirmed to properly model the high-temperature electromechanical losses in piezoelectric materials, e.g. of the langasite group [23,66,67].

Total electromechanical losses in piezoelectric solid can be represented by a sum of electrical conductivity related losses ${Q_c}^{-1}$, anelastic defect relaxation ${Q_a}^{-1}$, temperature-dependent background ${Q_T}^{-1}$, phonon-phonon interactions ${Q_{ph}}^{-1}$ and contributions, which are not dependent on temperature nor related to material losses and can be empirically termed as constant *C*. The latter models, for instance, the energy loss to electrodes and sample support, sample geometry factors, etc. Note that the piezoelectric effect couples electrical and mechanical systems and, thereby, the related losses. Consequently, the conductivity related losses ${Q_c}^{-1}$ stem from the motion of charge carriers with finite mobility in oscillating piezoelectric crystals. This loss component rapidly increases as the electrical conductivity of a piezoelectric material rises with temperature. Together with losses ${Q_a}^{-1}$ related to anelastic relaxation of defects in the crystals, the piezoelectric/conductivity losses ${Q_c}^{-1}$ are Debye functions of frequency and temperature, which implies that they reach peak values at a certain temperature for a given resonance frequency [65,66]:

$$Q_c^{-1}(\omega, T) = K^2 \frac{\omega\tau_c}{1 + \omega^2\tau_c^2}, \tag{5}$$

$$Q_a^{-1}(\omega, T) = \sum_{i=1}^{n} \frac{\Delta_{a,i}}{T} \frac{\omega\tau_{a,i}}{1 + \omega^2\tau_{a,i}^2}, \tag{6}$$

where $\omega = 2\pi f_r$ is the cyclic frequency, K^2 is the piezoelectric coupling factor, $\Delta_{a,i}$ are temperature-independent coefficients, proportional to concentration of defects in a solid, and τ are the relaxation times:

$$\tau_c = \frac{1}{2\pi f_\varepsilon} = \frac{\varepsilon_{ij}^S}{\sigma}, \tag{7}$$

$$\tau_{a,i} = \gamma_{a,i} \exp\left(\frac{U_{a,i}}{k_B T}\right). \tag{8}$$

Here f_ε is the dielectric relaxation frequency, σ is electrical conductivity, assuming the form of Eq. (3), ε_{ij}^S is dielectric permittivity at constant strain, $\gamma_{a,i}$ are temperature-independent time constants and $U_{a,i}$ are the activation energies of anelastic relaxation of defects. The coupling factor K^2 is determined by the piezoelectric constant e_{kl}, elastic constant at constant electric field c_{mn}^E and dielectric permittivity at constant strain:

$$K^2 = \frac{e_{kl}^2}{c_{mn}^E \varepsilon_{ij}^S}. \tag{9}$$

Using the above values from [53], coupling factors K^2 of 0.011 for LTE and RAD, 0.01 for TSM and 0.055 for TE resonance modes were applied in this analysis.

The solely temperature-dependent loss contributions with activation energy U_T assume an Arrhenius form with a temperature-independent coefficient Δ_T:

$$Q_T^{-1}(T) = \Delta_T \exp\left(\frac{-U_T}{k_B T}\right). \quad (10)$$

In general, this term has been so far not well understood and was a matter of disputes, which majorly lead to its attribution with thermally activated motion of dislocations contained in a crystalline solid [65,66]. However, the thermal background may be of different nature, which may include also other kinds of structural defects, to which no attribution were made in the literature by now. In the present study, the preliminary attempts of total Q^{-1} approximation yielded rather low values for ${Q_T}^{-1}$ in m-C+, c-OC and c-O, and this term has been excluded from further analysis of these samples. However, it appeared that for sample c-O+ the thermal background in the Arrhenius form must be included in the analysis.

Phonon-phonon interactions (PPI) are considered to be the limiting factor for a figure-of-merit *Qf* of a piezoelectric resonator. In the sub-gigahertz range these contributions are expected to be low and only weakly depend on temperature above 100 K [66,68]. If the *Qf* of single crystalline AlN is limited only by PPI, its value in the mega- to gigahertz frequency range is estimated to be 2.5×10^{13} Hz [68,69]. In the best case for the present study, the *Qf* product yields about 6.3×10^{12} Hz for 5th harmonic of TSM mode for m-C+, implying that the PPI-related contributions ${Q_{ph}}^{-1}$ to electromechanical losses may be excluded in the present analysis. Potentially, the measurement set-up or electrodes cause the constant or nearly constant loss contributions at moderate temperatures.

The results of analysis of $Q^{-1}(1/T)$ dependences for samples m-C+, c-O+, c-OC and c-O are illustrated in Fig. 6, and Table 4 provides the relevant parameters, obtained by fitting the corresponding curves to the sum

$$Q^{-1}(\omega,\ T) = Q_c^{-1}(\omega,\ T) + Q_a^{-1}(\omega,\ T) + Q_T^{-1}(T) + C. \quad (11)$$

Separation of temperature dependences of the total electromechanical losses occurring in the studied AlN samples allowed to identify the main loss contributions in them.

At high temperatures (T = 950–1200 K) in all of the studied AlN samples the electromechanical losses are majorly governed by the anelastic relaxation of mobile charge carriers (${Q_c}^{-1}$). Substituting in Eqs. (7) and (5) the experimental values of electrical conductivity and dielectric constants at high temperatures, obtained from EIS, one can estimate the expected conductivity-related electromechanical losses and the temperature, at which they reach the maximum. The temperature dependence of corresponding ${Q_c}^{-1}$ is shown in Fig. 6 by blue curves. For m-C+ and c-OC, the electromechanical losses rapidly increase at temperatures $T > 950$ K (Fig. 6, *a* and *b*), which fairly correlates with the rise of electrical conductivity of these crystals at $T > 900$ K (Fig. 2). Indeed, as can be seen on Fig. 6, *a* and *b*, the slopes of the high-temperature linear segments on the $\log(Q^{-1}) - T^{-1}$ dependences for losses estimated from EIS conductivity data (blue solid line) and those from Debye-fit of Q^{-1} (black dashed line) perfectly coincide. Furthermore, the values of activation energies E_a of 1.83 eV and 2.07 eV (Table 4), derived from the high-temperature peak in Q^{-1},

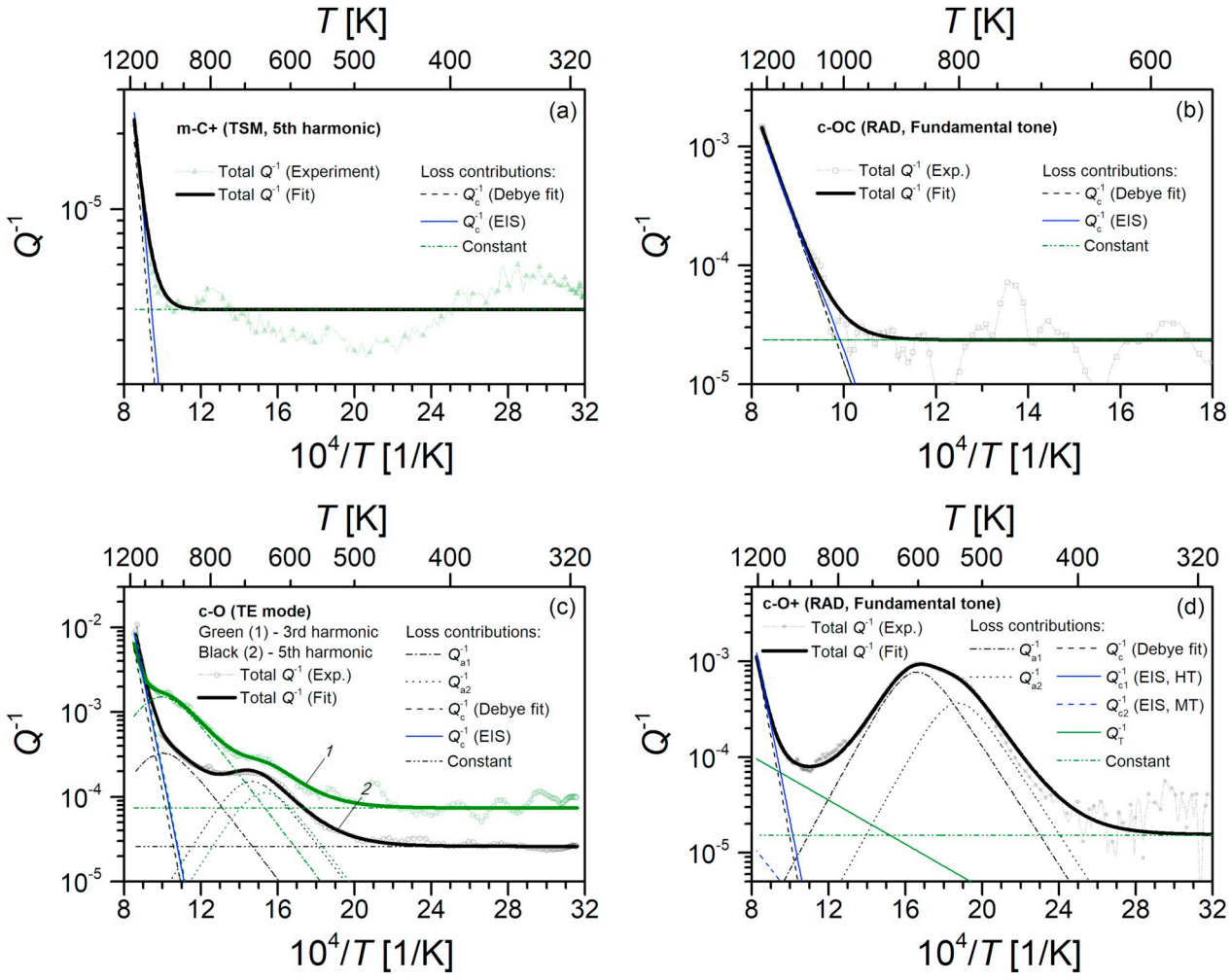

Fig. 6. Analysis of loss contributions in electromechanical properties of bulk AlN single crystals m-C+ (*a*, 5th harmonic TSM), c-OC (*b*, fundamental tone RAD), c-O (*c*, 3rd and 5th harmonic of TE), and c-O+ (*d*, fundamental tone RAD).

Table 4
Results of analysis of electromechanical losses in bulk AlN single crystals.

Parameter	m-C+	c-OC	c-O		c-O+
			3rd harmonic	5th harmonic	
ω (MHz)	120	8.67	155	259	8.98
K^2	0.01	0.011	0.055	0.055	0.011
σ_0 (S/m)	1360	2.01×10^4	6.04×10^6	1.96×10^7	5.04×10^4
E_a (eV)	1.83	2.07	2.256	2.260	2.13
Δ_{a1}	–	–	3.076	0.666	0.938
γ_{a1} (s)	–	–	4.42×10^{-12}	2.61×10^{-12}	3.987×10^{-13}
U_{a1} (eV)	–	–	0.643	0.641	0.656
Δ_{a2}	–	–	0.146	0.208	0.394
γ_{a2} (s)	–	–	7.89×10^{-14}	7.89×10^{-14}	7.242×10^{-14}
U_{a2} (eV)	–	–	0.641	0.640	0.659
Δ_T	–	–	–	–	8.505×10^{-4}
U_T (eV)	–	–	–	–	0.228
C	3.97×10^{-6}	2.36×10^{-5}	7.38×10^{-5}	2.61×10^{-5}	1.53×10^{-5}

are fairly consistent with E_a values, accordingly, provided for m-C+ and c-OC in Table 2. The pre-exponential factors σ_0 for these AlN crystals also closely match. Likewise, the conductivity-related loss component prevails at $T > 1000$ K in oxygen dominated AlN samples c-O+ and c-O (Figs. 6, *c* and *d*), for which the pre-exponential coefficients of $\sigma_0 = 5.04 \times 10^4$ S/m and $\sigma_0 \sim 10^6$ S/m (see Table 4) and the activation energies of $E_a = 2.13$ eV and $E_a = 2.26$ eV at $T = 900$–1200 K are in reasonable agreement with those derived from EIS measurements (Table 2).

As stated earlier, the thermal background did not need to be considered in the analysis of losses in m-C+, c-OC and c-O samples. However, the contribution must be included for sample c-O+ and is discussed based on results presented in [52]. Here, the background internal friction characteristic of grain boundary sliding (grain boundaries as a result of dislocations) has been excluded. Contrary, the broad peak spanning within 473–1473 K and exhibiting maximum at 1223 K has been related to anelastic electrical relaxation and considered to contribute in the background profile at moderate temperatures. The analysis indicates on point defects or their clusters as a possible origin of the electrical and mechanical relaxation in AlN, containing oxygen impurity. Further, a peak with lower activation energy of 0.78 eV (as compared to 1.32 eV for electrical relaxation at high temperatures) in the temperature range of 473–773 K with a maximum at 623 K was assigned with the losses due to mechanical anelastic relaxation.

The present studies show strong electromechanical losses in exactly the same temperature range. They are evident for c-O and c-O+ within $T = 400$–800 K, but are not observed for AlN with [O]/[C] ≤ 1. The time constants γ_a on the order of 10^{-13}–10^{-14} s obtained in this temperature range for samples c-O and c-O+ are fairly consistent with those expected for anelastic relaxation of point defects in solids [65]. To proof if these loss contributions could possibly be related with the electrical conductivity of AlN samples at moderate temperatures, the parameters σ_{02} and activation energies E_{a2} from Table 2 were inserted in Eqs. (7) and (5). The resulting curves for loss contributions are plotted for samples c-O and c-O+ as dashed blue lines in Fig. 6, *c* and *d*. As it can be seen, the anelastic relaxation of charge carriers in the temperature range of 400–800 K has little effect (c-O+) on the overall losses at moderate temperatures (for c-O, the estimated moderate-temperature Q_c^{-1} was well below 1×10^{-6}). Thus, the assumption about loss contributions from mechanical anelastic relaxation of point defects in these AlN samples appears to be quite appropriate. The large peak intensities Δ_a imply a high concentration of such defects in c-O and c-O+. Further, the peak splitting and close values of activation energies U_{a1} and U_{a2} may point on the formation of defect complexes, e.g. vacancy-impurity pairs, in them [65]. A key observation is the good match of time constants γ_{ai} and activation energies U_{ai} for both peaks of anelastic relaxation, observed on electromechanical losses of c-O sample at 3rd and 5th harmonics (Fig. 6, *c*). This implies that the observed peaks are not measurement artefacts, but a particular feature of this oxygen dominated AlN. Consistent with the increase of frequency from 3rd to 5th harmonic, the first anelastic maximum at $T \approx 950$ K shifts towards higher temperature for 5th harmonic and is, therefore, poorly visible due to the overlapping with loss contributions, related to charge carriers relaxation. Likewise, a little shift for the second peak at 650–700 K is observed for c-O sample, excited to 3rd and 5th harmonics of TE mode. However, since resonance measurements at higher harmonics have not been yet performed for c-O+, the existence and nature of the assumed defect complexes currently remain unclear. Remarkably, the activation energy and the time constants (see Table 4) for the second Q_{a2}^{-1} peak in c-O+ are comparable to those observed for the second peak in c-O sample, whereas time constants γ_{a1} do not differ much with those, determined for the first peak of anelastic relaxation in c-O sample. This observation points on, presumably, identical loss mechanisms in both samples, hence, also not excluding the contribution from defects of the same type and nature. Furthermore, the obtained U_a values of 0.64–0.66 eV for anelastic relaxation peaks are reasonably close to reported 0.78 eV in [52] or 0.65 eV in [38], which were related with aluminum vacancy – oxygen complexes. Accounting for the rise of Δ_{ai}, i.e. the concentration of anelastically relaxing defects, with oxygen content (Table 4), an assumption can be proposed that the observed loss peaks in c-O and c-O+ samples are indication of the presence of charged $V'''_{Al} - nO^{\bullet}_{N}$ point defect complexes in the studied AlN samples.

4. Conclusions

The studies of bulk AlN single crystals by means of resonant piezoelectric spectroscopy technique revealed considerable differences in the electromechanical losses in them, which appear to be strongly correlated to the relative content of growth-related electrically active impurities in the PVT-grown AlN. Modeling of temperature dependences of the electromechanical losses in the studied AlN crystals by a superposition of several Debye-functions allowed for assuming of the nature of main loss contributions. In aluminum nitride with oxygen content lower or comparable to that of carbon, the electrical conductivity was a major loss contribution in their resonant behavior at temperatures above 950 K. For oxygen-dominated AlN, strong contributions to electromechanical losses also at moderate temperatures were inherent, which can be attributed to anelastic relaxation of point defects or, potentially, their complexes contained in the crystals. The said point defects are, likely, present at relatively high concentrations in such AlN crystals. Meanwhile, the electrical conductivity σ_B of AlN with [O] ≈ [C] was the lowest, whereas with the increase of oxygen content in AlN, the σ_B and its activation energy increased from ca. 1.75–1.9 eV ([O] < [C]) up to 2.24 eV ([O]/[C] ≈ 1.8). In scope of possible

applications of AlN in high-temperature resonant devices, these observations point out on the necessity not only of reduction of the absolute concentration of growth-related impurities in AlN (in order to minimize conductivity-related losses), but also of careful adjustment of their relative content yet upon growth stage in order to minimize their adverse effects on electromechanical performance of AlN in a broad temperature range. The nature and type of the assumed defects in AlN is yet to be clarified though.

Declaration of competing interest

The authors declare that they have no known competing financial interests or personal relationships that could have appeared to influence the work reported in this paper.

Acknowledgements

A research grant from the German Research Foundation supported this work. Further, the authors from Clausthal University of Technology acknowledge the support of the Energie-Forschungszentrum Niedersachsen, Goslar, Germany.

References

[1] G. Yu, Aluminum nitride (AIN), in: M. Levinshtein, S. Rumyantsev, M. Shur (Eds.), Properties of Advanced Semiconductors, John Wiley & Sons, 2001(chap. 2).
[2] T. Aubert, J. Bardong, O. Legrani, O. Elmazria, M. Badreddine Assouar, G. Bruckner, A. Talbi, In situ high-temperature characterization of AlN-based surface acoustic wave devices, J. Appl. Phys. 114 (2013) 014505.
[3] M. Zhang, J. Yang, C. Si, G. Han, Y. Zhao, J. Ning, Research on the piezoelectric properties of AlN thin films for MEMS applications, Micromachines-Basel 6 (2015) 1236–1248.
[4] O. Mareschal, S. Loiseau, A. Fougerat, L. Valbin, G. Lissorgues, S. Saez, C. Dolabdjian, R. Bouregba, G. Poullain, Piezoelectric aluminum nitride resonator for oscillator, IEEE Trans. Ultrason. Ferroelectr. Freq. Control 56 (3) (2010) 513–517.
[5] X. Jiang, K. Kim, S. Zhang, J. Johnson, G. Salazar, High-temperature piezoelectric sensing, Sensors-Basel 14 (2014) 144–169.
[6] T. Aubert, O. Elmazria, J. Bardong, G. Bruckner, B. Assouar, Is AlN/sapphire bilayer structure an alternative to Langasite for ultra-high-temperature SAW applications? 2011 IEEE International Ultrasonics Symposium Proceedings, IEEE, Piscataway, 2011, p. 2082.
[7] S. González-Castilla, J. Olivares, E. Iborra, M. Clement, J. Sangrador, J. Malo, I. Izpura, Piezoelectric microresonators based on aluminium nitride for mass sensing applications, IEEE SENSORS 2008 Conference Proceedings, IEEE, Piscataway, 2008, p. 486.
[8] L. Berger, Semiconductor Materials, CRC Press, Boca Raton, FL, 1997.
[9] General properties of nitrides, in: H. Morkoç (Ed.), Handbook of Nitride Semiconductors and Devices, Volume 1, Materials Properties, Physics and Growth, WILEY-VCH Verlag GmbH & Co. KGaA, 2008(chap. 1).
[10] Q. Xia, H. Xia, A.L. Ruoff, Pressure-induced rocksalt phase of aluminum nitride: a metastable structure at ambient condition, J. Appl. Phys. 73 (1993) 8198.
[11] Y. Zhang, P. Franke, D. Li, H.J. Seifert, Lattice stability of metastable AlN and wurtzite-to-rock-salt structural transformation by CALPHAD modeling, Mater. Chem. Phys. 184 (2016) 233–240.
[12] M.R. Schwarz, et al., Formation and properties of rocksalt-type AlN and implications for high pressure phase relations in the system Si–Al–O–N, High Pressure Res. 34 (1) (2014) 22–38.
[13] A. Bellosi, E. Landi, A. Tampieri, Oxidation behavior of aluminum nitride, J. Mater. Res. 8 (3) (1993) 565.
[14] D.A. Parks, S. Zhang, B.R. Tittmann, High-temperature (> 500°C) ultrasonic transducers: an experimental comparison among three candidate piezoelectric materials, IEEE Trans. Ultrason. Ferroelectr. Freq. Control 60 (5) (2013) 1010–1015.
[15] A. Jacquot, B. Lenoir, A. Dauscher, P. Verardi, F. Craciun, M. Stölzer, M. Gartner, M. Dinescu, Optical and thermal characterization of AlN thin films deposited by pulsed laser deposition, Appl. Surf. Sci. 186 (1–4) (2002) 507–512.
[16] R. Rounds, B. Sarkar, A. Klump, C. Hartmann, T. Nagashima, R. Kirste, A. Franke, M. Bickermann, Y. Kumagai, Z. Sitar, R. Collazo, Thermal conductivity of single-crystalline AlN, Appl. Phys. Express 11 (2018) 071001.
[17] K.M. Rabe, C.H. Ahn, J.-M. Triscone (Eds.), Physics of Ferroelectrics, A Modern Perspective, Topics in Applied Physics, 104 Springer-Verlag, Berlin Heidelberg, 2007.
[18] G. Ohlendorf, D. Richter, J. Sauerwald, H. Fritze, High-temperature electrical conductivity and electro-mechanical properties of stoichiometric lithium niobate, Diffus. Fundam. 8 (2008) 6.1–6.7.
[19] X. Fu, E. Villora, Y. Matsushita, Y. Kitanaka, Y. Noguchi, M. Miyayama, K. Shimamura, N. Ohashi, Influence of growth conditions on the optical, electrical resistivity and piezoelectric properties of $Ca_3TaGa_3Si_2O_{14}$ single crystals, J. Ceram. Soc. Jpn. 124 (5) (2016) 523.
[20] S. Zhang, F. Yu, Piezoelectric materials for high temperature sensors, J. Am. Ceram. Soc. 94 (10) (2011) 3153.
[21] Y. Suhak, W.L. Johnson, A. Sotnikov, H. Schmidt, H. Fritze, Transport and electromechanical properties of $Ca_3TaGa_3Si_2O_{14}$ piezoelectric crystals at extreme temperatures, MRS Advances 1–7 (2019), https://doi.org/10.1557/adv.2019.16.
[22] Y. Suhak, M. Schulz, H. Wulfmeier, W.L. Johnson, A. Sotnikov, H. Schmidt, S. Ganschow, D. Klimm, H. Fritze, Langasite-type resonant sensors for harsh environments, MRS Advances 1 (21) (2016) 1513.
[23] Y. Suhak, M. Schulz, W.L. Johnson, A. Sotnikov, H. Schmidt, H. Fritze, Electromechanical properties and charge transport of $Ca_3TaGa_3Si_2O_{14}$ (CTGS) single crystals at elevated temperatures, Solid State Ionics 317 (2018) 221–228.
[24] T. Kim, J. Kim, R. Dalmau, R. Schlesser, E. Preble, X. Jiang, High-temperature electromechanical characterization of AlN single crystals, IEEE Trans. Ultrason. Ferroelectr. Freq. Control 62 (10) (2015) 1880–1887.
[25] M. Bickermann, B.M. Epelbaum, A. Winnacker, Characterization of bulk AlN with low oxygen content, J. Cryst. Growth 269 (2–4) (2004) 432–442.
[26] C. Hartmann, A. Dittmar, J. Wollweber, M. Bickermann, Bulk AlN growth by physical vapour transport, Semicond. Sci. Technol. 29 (2014) 084002.
[27] R.T. Bondokov, S.G. Mueller, K.E. Morgan, G.A. Slack, S. Schujman, M.C. Wood, J.A. Smart, L.J. Schowalter, Large-area AlN substrates for electronic applications: an industrial perspective, J. Cryst. Growth 310 (2008) 4020–4026.
[28] P. Lu, R. Collazo, R.F. Dalmau, G. Durkaya, N. Dietz, B. Raghothamachar, M. Dudley, Z. Sitar, Seeded growth of AlN bulk crystals in m- and c-orientation, J. Cryst. Growth 312 (2009) 58–63.
[29] Z.G. Herro, D. Zhuang, R. Schlesser, Z. Sitar, Growth of AlN single crystalline boules, J. Cryst. Growth 312 (2010) 2519–2521.
[30] R. Dalmau, Z. Sitar, AlN bulk crystal growth by physical vapor transport, in: G. Dhanaraj, K. Byrappa, V. Prasad, M. Dudley (Eds.), Springer Handbook of Crystal Growth, Springer Verlag, 2010(chap. 24).
[31] C. Hartmann, J. Wollweber, S. Sintonen, A. Dittmar, L. Kirste, S. Kollowa, K. Irmscher, M. Bickermann, Preparation of deep UV transparent AlN substrates with high structural perfection for optoelectronic devices, CrystEngComm 18 (2016) 3488.
[32] B. Raghothamachar, Y. Yang, R. Dalmau, B. Moody, S. Craft, R. Schlesser, M. Dudley, Z. Sitar, Defect generation mechanisms in PVT-grown AlN single crystal boules, Mat. Sci. Forum 740 (2013) 91–94.
[33] T. Zhou, B. Raghothamachar, F. Wu, R. Dalmau, B. Moody, S. Craft, R. Schlesser, M. Dudley, Z. Sitar, Characterization of threading dislocations in PVT-grown AlN substrates via X-ray topography and ray tracing simulation, J. Electron. Mater. 43 (4) (2014) 838–842.
[34] M. Bickermann, B.M. Epelbaum, O. Filip, P. Heimann, S. Nagata, A. Winnacker, Structural properties of aluminum nitride bulk single crystals grown by PVT, Phys. Status Solidi C 5 (6) (2008) 1502–1504.
[35] M. Bickermann, S. Schimmel, B.M. Epelbaum, O. Filip, P. Heimann, S. Nagata, A. Winnacker, Structural defects in aluminium nitride bulk crystals visualized by cathodoluminescence maps, Phys. Status Solidi C 8 (7–8) (2011) 2235–2238.
[36] M. Bickermann, B.M. Epelbaum, O. Filip, P. Heimann, S. Nagata, A. Winnacker, Point defect content and optical transitions in bulk aluminum nitride crystals, Phys. Status Solidi B 246 (6) (2009) 1181–1183.
[37] B.E. Gaddy, Z. Bryan, I. Bryan, R. Kirste, J. Xie, R. Dalmau, B. Moody, Y. Kumagai, T. Nagashima, Y. Kubota, T. Kinoshita, A. Koukitu, Z. Sitar, R. Collazo, D.L. Irving, Vacancy compensation and related donor-acceptor pair recombination in bulk AlN, Appl. Phys. Lett. 103 (2013) 161901.
[38] A.Y. Polyakov, N.B. Smirnov, A.V. Govorkov, T.G. Yugova, K.D. Scherbatchev, O.A. Avdeev, T.Yu. Chemekova, E.N. Mokhov, S.S. Nagalyuk, H. Helava, Yu.N. Makarov, Deep centers in bulk AlN and their relation to low-angle dislocation boundaries, Physica B 404 (2009) 4939–4941.
[39] C. Guguschev, E. Moukhina, J. Wollweber, A. Dittmar, K. Böttcher, C. Hartmann, S. Golka, R. Fornari, In situ kinetic investigations during aluminium nitride purification and crystal growth processes by capillary coupled mass spectrometry, Thermochim. Acta 526 (1–2) (2011) 213.
[40] R. Collazo, J. Xie, B.E. Gaddy, Z. Bryan, R. Kirste, M. Hoffmann, R. Dalmau, B. Moody, Y. Kumagai, T. Nagashima, Y. Kubota, T. Kinoshita, A. Koukitu, D.L. Irving, Z. Sitar, On the origin of the 265nm absorption band in AlN bulk crystals, Appl. Phys. Lett. 100 (2012) 191914.
[41] D. Alden, J.S. Harris, Z. Bryan, J.N. Baker, P. Reddy, S. Mita, G. Callsen, A. Hoffmann, D.L. Irving, R. Collazo, Z. Sitar, Point-defect nature of the ultraviolet absorption band in AlN, Phys. Rev. Applied 9 (2018) 054036.
[42] J.S. Harris, J.N. Baker, B.E. Gaddy, I. Bryan, Z. Bryan, K.J. Mirrielees, P. Reddy, R. Collazo, Z. Sitar, D.L. Irving, On compensation in Si-doped AlN, Appl. Phys. Lett. 112 (2018) 152101.
[43] R.W. Francis, W.L. Worrell, High temperature electrical conductivity of aluminum nitride, J. Electrochem. Soc. 123 (3) (1976) 430–433.
[44] K. Irmscher, C. Hartmann, C. Guguschev, M. Pietsch, J. Wollweber, M. Bickermann, Identification of a tri-carbon defect and its relation to the ultraviolet absorption in aluminum nitride, J. Appl. Phys. 114 (2013) 123505.
[45] I.A. Weinstein, A.S. Vokhmintsev, D.M. Spiridonov, Thermoluminescence kinetics of oxygen-related centers in AlN single crystals, Diam. Relat. Mater. 25 (2012) 59–62.
[46] T. Mattila, R.M. Nieminen, Ab initio study of oxygen point defects in GaAs, GaN, and AlN, Phys. Rev. B 54 (23) (1996) 16676.
[47] C. Stampfl, C.G. Van de Walle, Theoretical investigation of native defects, impurities, and complexes in aluminum nitride, Phys. Rev. B 65 (2002) 155212.
[48] Q. Yan, A. Janotti, M. Scheffler, C.G. Van de Walle, Origins of optical absorption

and emission lines in AlN, Appl. Phys. Lett. 105 (2014) 111104.
[49] A. Uedono, S. Ishibashi, S. Keller, C. Moe, P. Cantu, T.M. Katona, D.S. Kamber, Y. Wu, E. Letts, S.A. Newman, S. Nakamura, J.S. Speck, U.K. Mishra, S.P. DenBaars, T. Onuma, S.F. Chichibu, Vacancy-oxygen complexes and their optical properties in AlN epitaxial films studied by positron annihilation, J. Appl. Phys. 105 (2009) 054501.
[50] V.L. Richards, T.Y. Tien, R.D. Pehlke, High-temperature electrical conductivity of aluminum nitride, J. Mater. Sci. 22 (1987) 3385–3390.
[51] O. Elmazria, M.B. Assouar, P. Renard, P. Alnot, Electrical properties of piezoelectric aluminium nitride films deposited by reactive dc magnetron sputtering, Phys. Status Solidi A 196 (2) (2003) 416–421.
[52] J.C. Goldsby, Micro-mechanical and electrical properties of monolithic aluminum nitride at high temperatures, J. Alloys Compd. 321 (2001) 67–71.
[53] A.V. Sotnikov, H. Schmidt, M. Weihnacht, E.P. Smirnova, T.Y. Chemekova, Y. Makarov, Elastic and piezoelectric properties of AlN and $LiAlO_2$ single crystals, IEEE Trans. Ultrason. Ferroelectr. Freq. Control 57 (4) (2010) 808–811.
[54] H. Fritze, High-temperature bulk acoustic wave sensors, Meas. Sci. Technol. 22 (2011) 012002.
[55] T. Schneider, D. Richter, S. Doerner, H. Fritze, P. Hauptmann, Novel impedance interface for resonant high-temperature gas sensors, Sensors Actuators B Chem. 111–112 (2005) 187–192.
[56] R.H. Olsson III, K.E. Wojciechowski, D.W. Branch, Origins and mitigation of spurious modes in aluminum nitride microresonators, in: Proc. IEEE Int. Ultrason. Symp., Oct. 2010, pp. 1272–1276.
[57] D.W. Branch, K.E. Wojciechowski, R.H. Olsson, Elucidating the origin of spurious modes in aluminum nitride microresonators using a 2-D finite-element model, IEEE Trans. Ultrason. Ferroelectr. Freq. Control 61 (5) (2014) 729–738.
[58] R. Abdolvand, B. Bahreyni, J.E.-Y. Lee, F. Nabki, Micromachined resonators: a review, Micromachines-Basel 7 (2016) 160.
[59] IEEE Standard on Piezoelectricity. ANSI/IEEE Standards, 176 (1987), pp. 1–66.
[60] S.A. Jang, G.M. Choi, Electrical conduction in aluminum nitride, J. Am. Ceram. Soc. 76 (4) (1993) 957–960.
[61] H.-K. Lee, H.M. Lee, D.K. Kim, AC impedance spectroscopy of CaF_2-doped AlN ceramics, J. Am. Ceram. Soc. 97 (3) (2014) 805–810.
[62] Piezoelectric ceramic resonators (resonance frequency and equivalent electrical circuit), in: J. Erhart, P. Půlpán, M. Pustka (Eds.), Piezoelectric Ceramic Resonators, Springer International Publishing, 2017(chap. 3).
[63] J. Erhart, L. Rusin, L. Seifert, Resonant frequency temperature coefficients for the piezoelectric resonators working in various vibration modes, J. Electroceram. 19 (2007) 403–406.
[64] G. Wang, L.-X. Xu, A. Ababneh, P. Schwarz, D. Feili, H. Seidel, AlN micro-mechanical radial-contour disc resonator, J. Micromech. Microeng. 23 (2013) 095002.
[65] A.S. Nowick, B.S. Berry, Anelastic Relaxation in Crystalline Solids, Academic, New York, NY, 1972.
[66] W.L. Johnson, S.A. Kim, S. Uda, C.F. Rivenbark, Contribution to anelasticity in langasite and langatate, J. Appl. Phys. 110 (2011) 123528.
[67] W.L. Johnson, M. Schulz, H. Fritze, Acoustic and Electrical Properties of $Ca_3TaGa_3Si_2O_{14}$ Piezoelectric Resonators at Elevated Temperatures. https::://doi.org/10.1109/ICSENS.2013.6688573.
[68] R. Tabrizian, M. Rais-Zadeh, F. Ayazi, Effect of phonon interactions on limiting the f.Q product of micromechanical resonators, Transducers 2009, Denver, CO, USA, June 21–25, 2009, p. 2131–2134.
[69] S. Ghaffari, S.A. Chandorkar, S. Wang, E.J. Ng, C.H. Ahn, V. Hong, Y. Yang, T.W. Kenny, Quantum limit of quality factor in silicon micro and nano mechanical resonators, Sci. Rep. 3 (2013) 3244, https://doi.org/10.1038/srep03244.